Electronic Supplementary Material (ESI) for Nanoscale.

Imaging dopant distribution across complete phase transformation by TEM and upconversion emission

Daniel Avram[a], Claudiu Colbea[a], Mihaela Florea[b], Sorin Lazar[c], Daniel Stroppa[c] and Carmen Tiseanu*[a]

[a]National Institute for Laser, Plasma and Radiation Physics, P.O. Box MG-36, RO 76900, Bucharest-Magurele, Romania

[b]National Institute of Materials Physics, 405A Atomistilor Street, 077125 Magurele-Ilfov, Romania

[c]Thermo Fisher Scientific, Achtseweg Noord 5, 5651 GG Eindhoven, The Netherlands

Corresponding Author

*Author to whom correspondence should be addressed.

Electronic mail: carmen.tiseanu@inflpr.ro

Materials and Methods

Materials

The Er, Li doped ZrO_2 nanoparticles were prepared via an efficient and low cost method, known as citrate complexation method. In a typical synthesis, aqueous metal nitrates solutions are mixed with citric acid, in molar ratio of 1:1.2, and stirred for one hour at a constant temperature of 60 °C. The resulting solution is evaporated in a vacuum rotavapor at 60 °C until a gel was obtained. The gel was dried at 60 °C for 5 hours in an oven with vacuum and at 120 °C without the vacuum overnight. For the surface Li impregnation, the powder from the same aliqot of doped 3% Er-ZrO_2 was used for all three Li concentration (5,10 and 15%) in order to have the same Er distribution. Then, the dried 3% Er-ZrO_2 powder was added to a water-based solution containing the corresponding amount of $LiNO_3$ and stirred at room temperature for 1 h. After filtration, the solid is dried at 120 °C over night. Afterwards, all four samples were calcined at 750 °C for 4 hours at a heating rate/cooling rates of 5 °C/min. Additional Li free, Er doped ZrO_2 were obtained by the same citrate method described above with Er molar concentration of 1, 3, 5, 7, 10% followed by calcination at 750 °C for 4 hours at a heating rate/cooling rates of 5 °C/min and used as tetragonal reference samples. The 1% Er-ZrO_2 is fully transformed into monoclinic phase following calcination at 1000 °C and used as a monoclinic reference sample. Additional series of 3%Eu, Li (0, 5, 10 and 15%) by use of similar synthetic route as used for 3Er, Li series except that Er was replaced by Eu.

Characterization

Powder X-ray diffraction (XRD) patterns were recorded on a Bruker-AXS D8 Advance diffractometer equipped with a one-dimensional detector (LynxEye type) using Cu-Kα radiation

(0.1541 nm) at a scanning speed of 0.04 degrees min^{-1} in the 10 - 80 degrees 2θ range with a collection time of 1s per step. Rietveld refinement was not attempted.

Particle size were determined using Scherrer equation, where λ is the wavelength in nanometer, β is the peak width of the diffraction peak profile at half maximum height resulting from small crystallite size in radians, K is the shape factor which was considered 0.9 in our study and θ is the Bragg angle $D = \frac{K\lambda}{\beta \cos\theta}$. For the phase content we used MAUD software (http://maud.radiographema.eu) which requires the CIF data files (COD ID:1522143 for the monoclinic zirconia and for the tetragonal zirconia (Cod ID: 2300612) based on RITA/RISTA methodS[1] as well as the Toraya methods.S[2] Toraya method estimates the volumetric fractions of the monoclinic ZrO_2 (Vm) and tetragonal ZrO_2 (Vt) phases from the intensities of the diffraction peaks as (-111) and (111) of monoclinic ZrO_2 and line diffraction (101) of tetragonal ZrO_2 as $Vm = \frac{1.311x}{1+0.311x}$ where $x = \frac{Im(-111)+Im(111)}{Im(-111)+Im(111)+It(101)}$; The tetragonal fraction can be calculated as $Vt = 1 - Vm$.

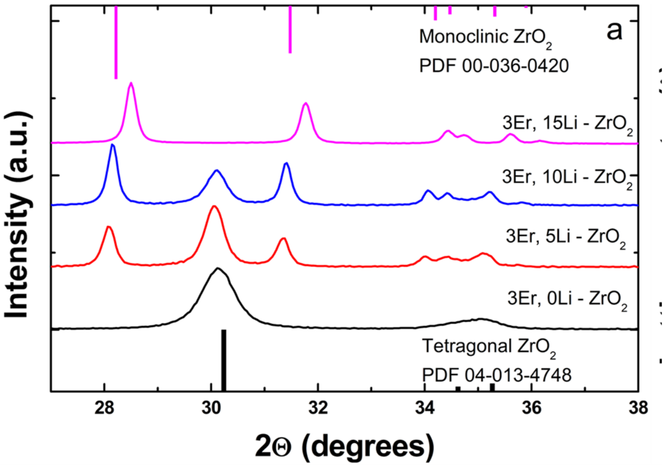

Figure S1. (a) Enlarged region of XRD patterns of 3Er, Li series.

As illustrated in Figure S1, with the increase of Li concentration, monoclinic XRD (111) peak shifts toward larger angles, from 31.363 (5%Li) to 31.404 (10%Li) to 31.764 (15%Li). In opposition, the tetragonal (101) XRD reflection shifts smaller angle from 30.12 (0%Li) to 30.07(5%Li) followed by a reverse shift at 30.112(10%Li).

Table S1 Ionic radii of Er, Li and Zr (nominal charges of 3+, 1+ and 4+) in the 8- and 7-fold coordination sites corresponding to tetragonal and monoclinic phase, respectively.

Metal	Ionic radii (Å)	
	8-fold coordination (tetragonal)	7-fold coordination (monoclinic)
Li +	0.92	-
Er3+	1.004	0.945
Zr4+	0.84	0.78

Microbeam X-ray fluorescence (micro-XRF) spectrometry was performed on a custom-made instrument with an X-ray tube: Oxford Instruments, Apogee 5011, Mo target, focus spot ~40 µm, max. high voltage - 50 kV, max current - 1 mA, Amptek X-123 complete X-Ray spectrometer with Si - PIN detector. Attenuated total reflection-Fourier transform infrared (ATR-FTIR) spectra were measured on a Spectrum Two, PerkinElmer spectrometer using an ATR device with a diamond crystal plate (Pike Technologies, Madison, WI). Spectra were recorded at 4 cm^{-1} nominal resolution and 100 scans. Raman analysis was carried out with a Horiba Jobin Yvon - Labram HR UV-Visible-NIR Raman Microscope Spectrometer at 488 nm. Attenuated total reflection-Fourier transform infrared (ATR-FTIR) spectra were measured on a Spectrum Two, PerkinElmer spectrometer using an ATR device with a diamond crystal plate (Pike Technologies, Madison, WI). Spectra were recorded at 4 cm^{-1} nominal resolution and 100 scans.

Electron microscopy samples were prepared by dispersing the Er, Li-doped ZrO_2 nanocrystalline powders in absolute ethanol with aid of a low-power ultrasonic bath at room temperature and dripping the dispersions onto copper grids covered with a thin amorphous carbon film.

TEM characterization was performed using a Thermo Fisher Scientific Themis Z microscope equipped with Schottky field-emission electron gun operating at 300 kV and with both probe and image aberration-correctors. Scanning transmission electron microscopy (STEM) imaging was carried out with a 50 pA electron beam with 20 mrad convergence angle. High angle annular dark field (HAADF) were obtained with a collection angle ranging from 68 to 200 mrad, while integrated differential phase contrast (iDPC)[S2] were collected within a 8 -32 mrad range. Energy-dispersive X-ray spectroscopy (EDX) measurements were carried in STEM mode with a 0.5 nA electron beam and using a 4-detectors collection setup with 0.7 srad collection range. Automated STEM-EDX tomography experiments were carried out within a -60^{o} to $+65^{o}$ tilt range with a 5^{o} degrees tilt step, and the tomograms obtained by imaging and chemical mapping were reconstructed using a 30-iteration simultaneous iterative reconstruction technique (SIRT) workflow implemented on Inspect3D software.

Luminescence measurements:

Phase selective time-resolved up-conversion emission spectra were recorded at room temperature using a wavelength tunable pulsed laser (210 ÷ 2300 nm), NT340 Series EKSPLA OPO (Optical Parametric Oscillator) as excitation source operated at 10 Hz with narrow bandwidth (around 5 cm^{-1}) and short pulse width (<5 ns) and for cw up-conversion emission, a 980 nm continuous-wave (cw) fiber coupled diode laser system (RLTMFC-980-4W-5, ROITHNER LASERTECHNIK GmbH) with a bandwidth of ~5nm was used. For the fiber coupled laser diode, the power was 1.3 W with 10.6 W/cm^2 power density and for the OPO laser system, at 950 - 990 nm range, the energy per laser pulse was ~5 mJ with an average power density of ~400 mW/cm^2. As detection system, an intensified CCD (iCCD) camera (Andor Technology, iStar iCCD DH720) coupled to a spectrograph (Shamrock 303i, Andor) was used. The detection range of the iCCD is 300 - 870 nm. Photoluminescence was detected with a spectral resolution of 0.44 nm and the input slit of the spectrograph was set to 10 μm. The temperature of the iCCD was lowered to -20 °C to improve its signal to noise ratio. For the comparison of the up-conversion emission intensity, the laser power density was kept constant to 250 mW/cm^2. The powder samples were placed in the same geometrical configuration on a solid sample holder (sample holder area of 14 mm X 7 mm, from Horiba Scientific, J1933) in reflection mode using the same quantity of nanoparticles on all samples yielding the same excitation conditions (same energy density distribution on the samples).

Up-conversion emission spectra. The up-conversion emission spectra upon OPO pulsed laser excitation were recorded using the same input slit (10 μm), exposure time (gate width of 0.5 ms), delay after the laser pulse (0.5 μs) and MCP gain (100). The up-conversion emission spectra upon cw laser diode excitation at 980 nm were recorded using the same input slit (10 μm), exposure time (gate width of 100 ms). All the digital photos were obtained by use of a Canon EOS 60D camera with 400 ISO and different integration time in dark room conditions (1 to 15 s). For the 15Li sample, the integration time used to record the photograph was set to 15 s due to the lower emission intensity from this sample, while the rest of the sample images were recorded with a 1 s integration time. To detect the presence of minor surface/ segregated Er, the delay was set to 0.1 μs and the gate width was set to 10 μs, respectively. The weak intensity tetragonal emission measured with monoclinic 3Er, 15Li - ZrO_2 was detected by use of high MCP gain of 150 while the final spectrum was the result of 300 accumulated spectra.

Up-conversion excitation spectra. The up-conversion excitation spectra were constructed by integrating the emission area of interest: green emission for the monoclinic phase content (510 - 575 nm corresponding to $^2H_{11/2}$, $^4S_{3/2}$ - $^4I_{15/2}$ emission transition) and red emission (630 - 700 nm corresponding to $^4F_{9/2}$ - $^4I_{15/2}$ emission transition) under the same experimental conditions by scanning the laser excitation wavelength with a 1 nm step. The green and red emissions were measured by use of an intensified CCD (iCCD) camera (Andor Technology, iStar iCCD DH720) coupled to a spectrograph (Shamrock 303i, Andor).

Emission decays. Emission decays were measured for both upconversion and down-conversion excitation mode. Upconversion excitation refers to exciting nanoparticles with 980 nm light and monitoring emission from the Er $^2H_{11/2}$, $^4S_{3/2}$, and $^4F_{9/2}$ emitting states at 550 and 680 nm respectively. These states are populated *via* different upconversion mechanisms (ground state absorption followed by excited state absorption or energy transfer up-conversion mechanisms), and thus, measuring the lifetime of these states when excited by upconversion provides insight to the upconversion pathway. Whilst down-conversion excitation refers to directly exciting the states of interest to remove the convolution of the lifetimes of the intermediary states (usually with longer lifetime than the monitored emission) as for the upconversion processes.

For the emission decay measurements in visible range, it was used a PMT module (PMA-C 192-N-M, PicoQuant GmbH) with appropriate filters and a PCIe TCSPC card TimeHarp 260 NANO (PicoQuant GmbH) as acquisition system. For green emission, a 550 nm (± 10 nm) bandpass filter was used, whilst for red emission a pair formed by 750 nm short pass and 610 nm long pass filter was used to select the monitored emission wavelength.

The average decay lifetimes were estimated by integrating the area under the normalized emission decays: $\bar{\tau} = \int_0^\infty tI(t)dt / \int_0^\infty I(t)dt$, where $I(t)dt$ is the normalized decay law.

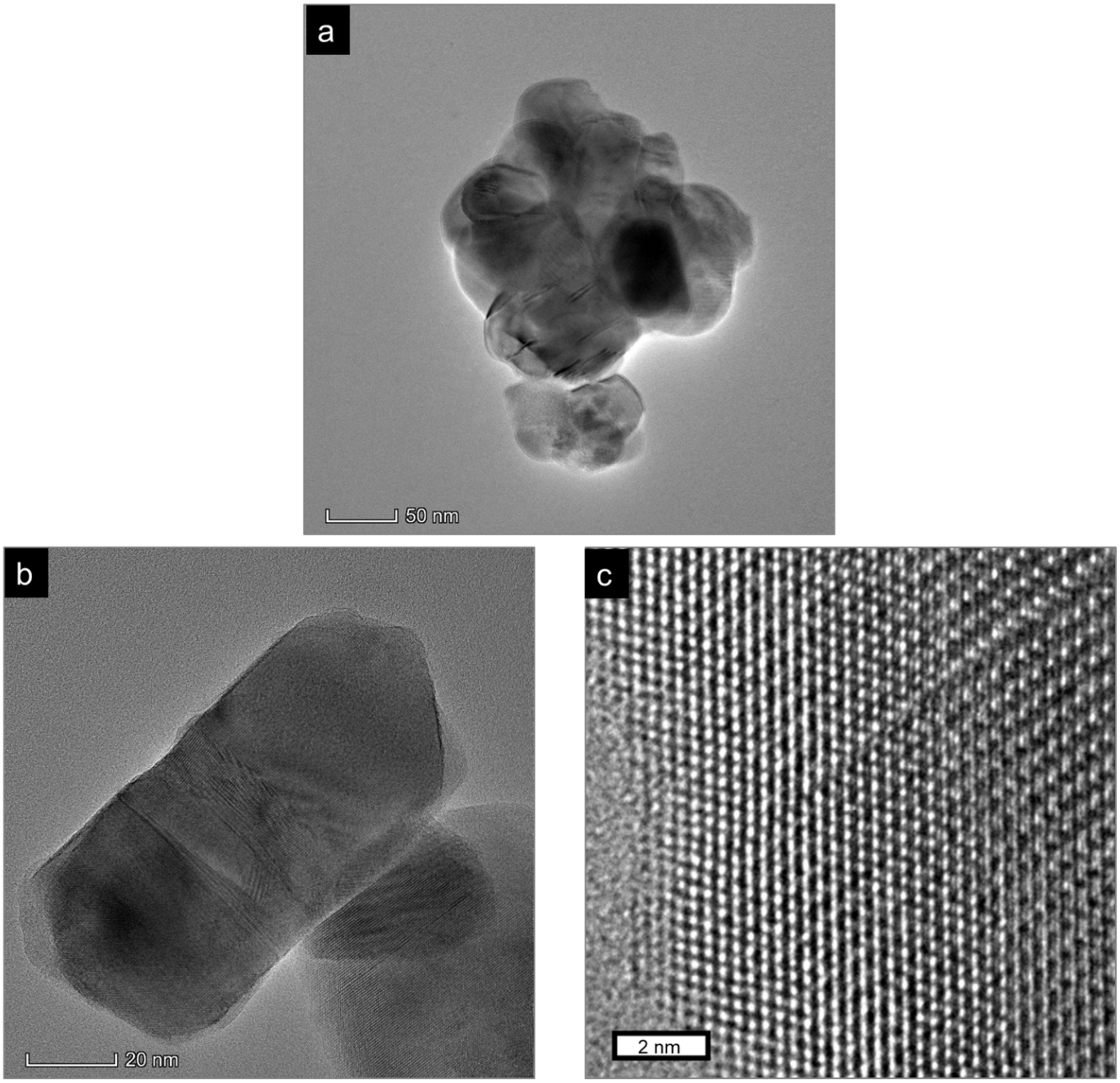

Figure S2. (a) TEM sample overview reveals the agglomeration state (3Er,15Li-ZrO_2). Individual particles have sizes within 20 – 80 nm range; (b) HRTEM image indicates sample crystallinity and presence of defects. Heterogeneous nanoparticles morphology is observed; (c) Digital zoom (10x) of previous HRTEM image, indicating the tip of a typical line defect at atomic resolution (scale bar: 2nm)

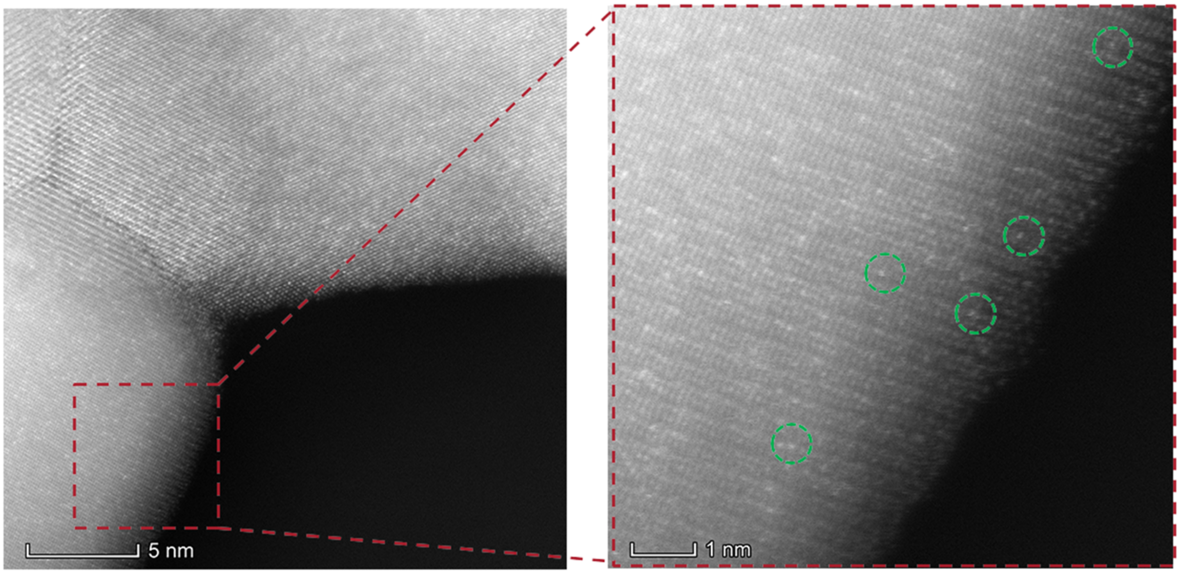

Figure S3. HAADF-STEM image of a grain interface of 3Er, 5Li- ZrO_2 showing Er substituting for Zr.

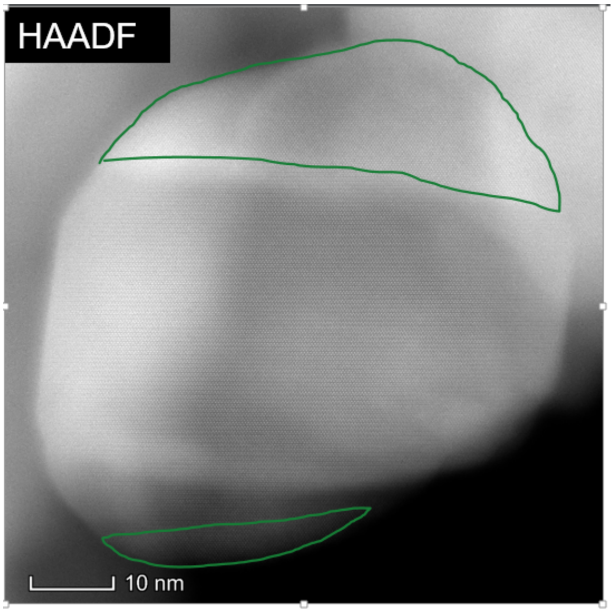

Figure S4. HAADF-STEM of 3Er, 10Li –ZrO_2. The green outline indicates the approximate contour of the identified ZrO_2 tetragonal phase regions (see **Figure 3** and discussion in the main text).

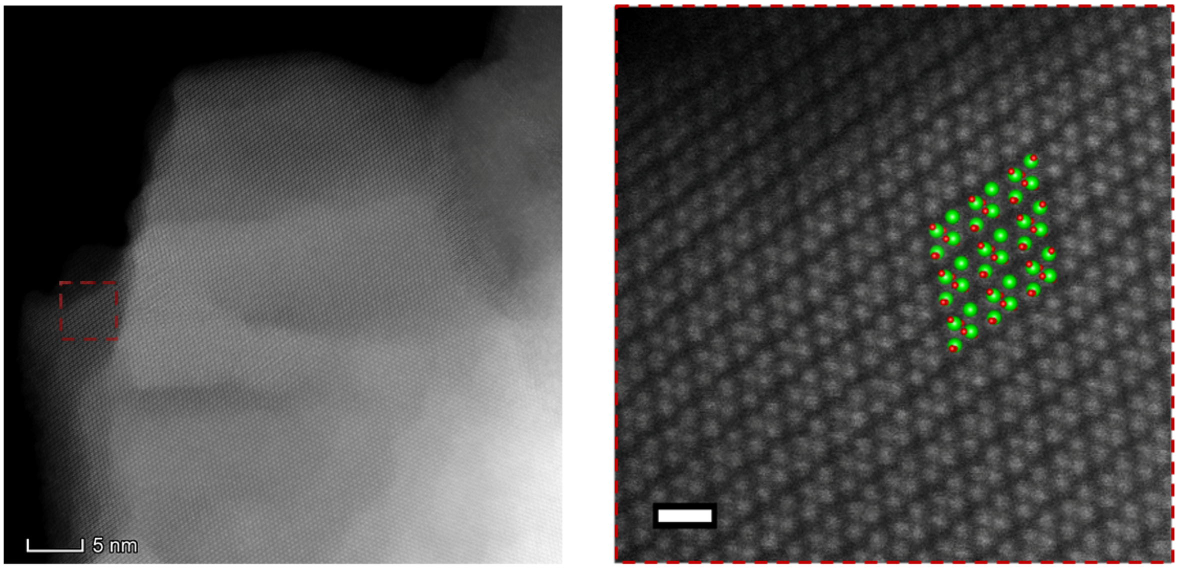

Figure S5. Atomic resolution HAADF-STEM images on selected nanograins of 3Er, 5Li-ZrO_2 with a monoclinic structure atomic model overlay (Zr-green, O-red).

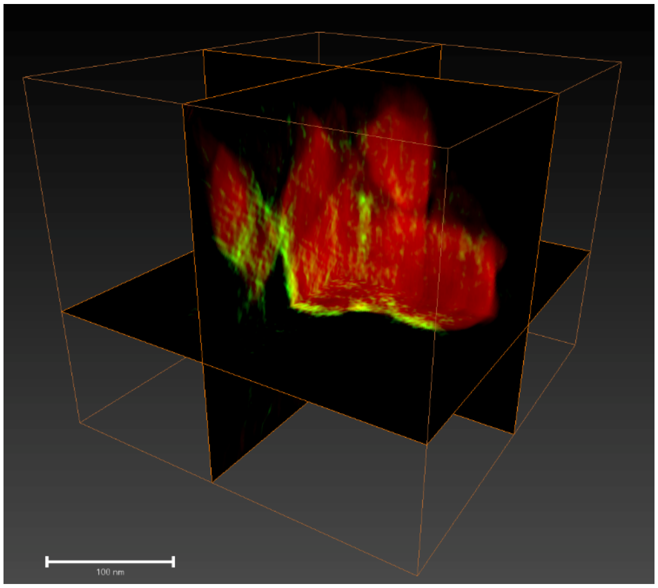

Figure S6. EDX tomography visualization from a small agglomerate of 3Er, 15Li- ZrO_2 nanocrystals. The color code refers to net EDX counts of Er (green) and Zr (red) chemical elements. This result evidences a significant surface segregation of Er dopant atoms. A more comprehensive visualization of the EDX tomography results is available in video format as a support file.

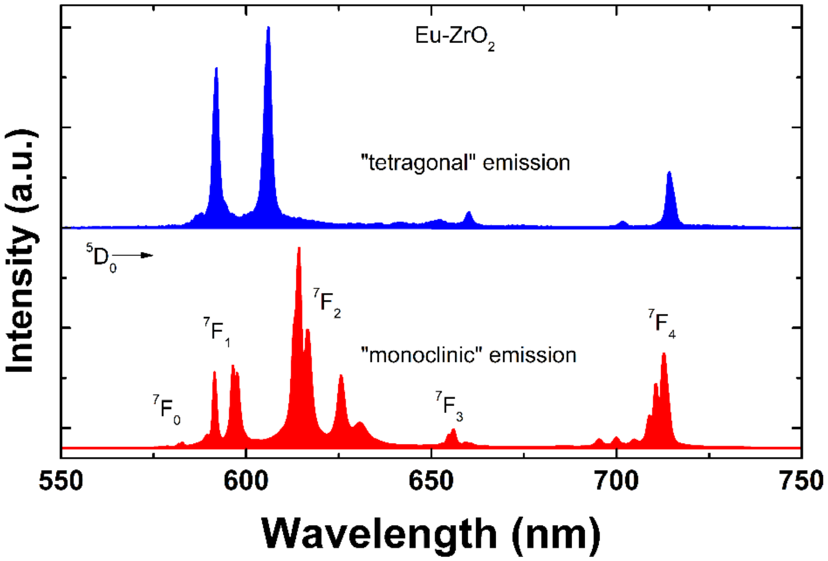

Figure S7. Fingerprint emission spectra of Eu in 3Eu, 0Li –ZrO_2 and 3Eu, 15 Li- ZrO_2. The emission spectra match the well-known shapes of Er in the tetragonal and monoclinic ZrO_2 reported in literature. The emission spectra of mixed phase 3Eu, 5Li and 3Eu, 10 Li-ZrO_2 display a spectral convolution of the two emission spectra (not shown).

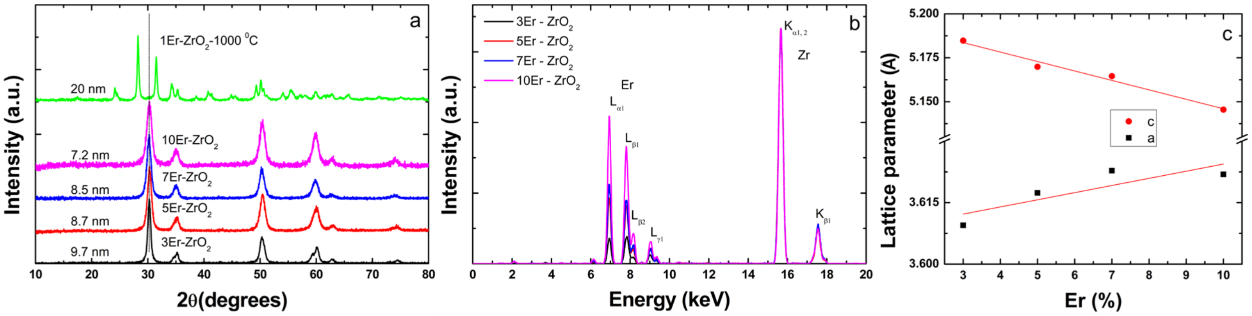

Figure S8. **(a)** XRD patterns and XRF spectra (b) of tetragonal and monoclinic Er- ZrO$_2$ reference series; (c) Dependency of a/ c lattice constants of tetragonal reference series on Er concentration.

Table S2. Lattice constants of 3-10 % Er-ZrO$_2$ tetragonal reference series and 1Er-ZrO$_2$ monoclinic reference sample.

Sample	phase	a (Å)	b (Å)	c (Å)	beta (°)	c/a	volume (Å^3)
3Er-ZrO$_2$	*t*	3.609	-	5.185	-	1.4364	67.549
5Er-ZrO$_2$	*t*	3.620	-	5.155	-	1.4275	67.735
7Er-ZrO$_2$	*t*	3.623	-	5.164	-	1.4256	67.783
10Er-ZrO$_2$	*t*	3.622	-	5.146	-	1.4206	67.490
1Er-ZrO$_2$	*m*	5.440	5.342	5.276	99.335	-	

Tetragonal ZrO_2 crystallizes in space group D_{4h}^{15} - $P4_2/nmc$ with Z=2. [S[3]] Er can substitute Zr without altering the crystal structure. The average Er−Er distance [S4] d in the tetragonal reference series (3-10) Er-ZrO_2 can be approximated by the cubic root of the corresponding unit cell volume divided by Z and the Er doping concentration percentage (x) over total cationic sites:

$$d_{Er-Er} = \left(\frac{a^2 c}{Zx}\right)^{1/3}$$

where a and c Å are the lattice parameters of the tetragonal unit cell (**Table S2**) with a volume of a^2c. The error in the lattice parameters is generally below 0.1%. Therefore, it is negligible here in comparison to the experimental uncertainty of the doping level. Differences in the lattice parameters due to the Er doping can be neglected as well.

Table S3. Average lifetimes monitoring the green emission at 560 nm of the monoclinic reference sample (1%Er-ZrO_2, excitation at 982 nm) and red emission at 560 nm of the tetragonal reference samples (3, 5, 7 and 10%Er-ZrO_2, excitation at 952 nm)

Sample	Average lifetime (ms) (±0.005 ms)
1Er-ZrO_2	0.159
3Er-ZrO_2	0.139
5Er-ZrO_2	0.107
7Er-ZrO_2	0.088
10Er-ZrO_2	0.039

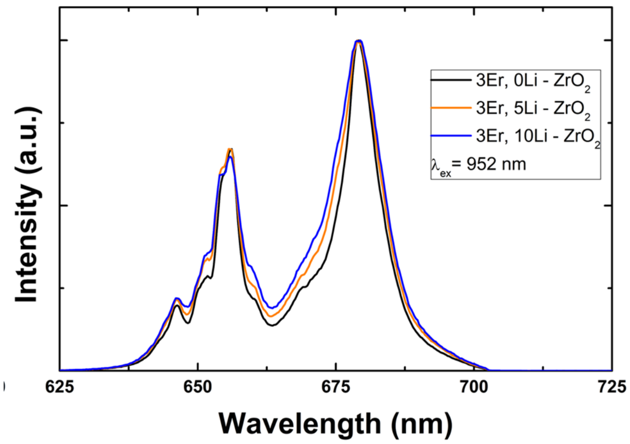

Figure S9. Li induced broadening of UPC emission spectra assigned to Er-Er enrichment in the tetragonal domains. All spectra were normalized at the maximum peak intensity of $^4F_{9/2}$ emission at 680 nm.

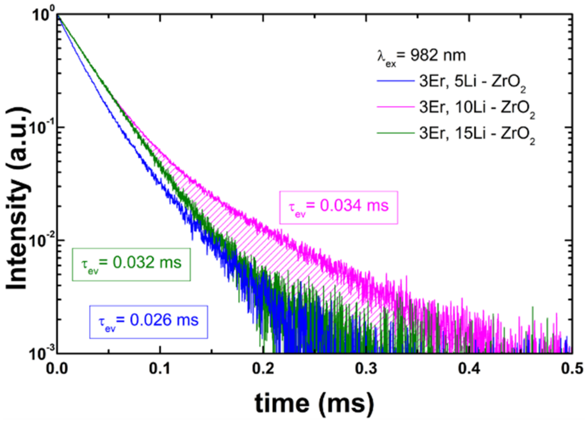

Figure S10. Comparison between the monoclinic phase UPC decays (excitation at 982 nm) monitoring the emission of $^4S_{3/2}$ green emitting level at 560 nm. The comparison highlights a close to monoexpoential shape for decay of the 3Er, 15 Li –ZrO_2 and “lifted” tails for the decays of 3Er, 5Li- ZrO_2 and 3Er, 10Li- ZrO_2.

References

S[1] L. Lutterotti, M. Bortolotti, G. Ischia, I. Lonardelli, H. Wenk, *Zeitschrift Fur Kristallographie* **2007**, 125.

S[2] H. Toraya, M. Yoshimura, S. Somiya, *Journal of the American Ceramic Society* **1984**, 67, C119.

S[3] G. Teufer, *Acta Crystallographica* **1962**, 15, 1187.